



# Low energy oxygen implantation induced improved crystallinity and optical properties of surface modified ZnO single crystals

P.K. Giri <sup>\*</sup>, Satchi Kumari, D.K. Goswami

Department of Physics, Indian Institute of Technology, Guwahati 781039, Assam, India

## ARTICLE INFO

Article history:  
Available online 27 May 2009

Keywords:  
ZnO  
Oxygen implantation  
Defects  
Photoluminescence  
RBS  
Raman

## ABSTRACT

We report on the low energy oxygen implantation induced improvement in crystallinity and optical properties of surface modified ZnO single crystals. Undoped ZnO (0 0 0 1) single crystal wafers are implanted with 100 keV oxygen ions at a dose of  $5 \times 10^{13}$  and  $5 \times 10^{14}$  cm<sup>-2</sup> and subsequently annealed at 500 and 600 °C in oxygen ambient. The as-implanted and annealed ZnO wafers are studied by Rutherford back scattering spectrometry (RBS), channeling, Raman, photoluminescence (PL), and Fourier transform infrared spectroscopy (FTIR). Channeling studies show a relatively high  $\chi_{\min}$  (>20%) in the virgin ZnO wafer. After implantation and two-step annealing, RBS studies show improved crystallinity. Raman line width analysis for the  $E_2^{\text{high}}$  mode indicates reduction in strain in the annealed samples as compared to the virgin ZnO wafer. As-implanted samples show drastic quenching of the near band-edge (NBE) PL band due to defects created by the implantation. However, after two-step annealing, the low-dose implanted sample show a five-fold increase in intensity ratio of NBE band (376 nm) to defect related broad band (~530 nm) at room temperature. Implantation induced changes in the composition and improved crystallinity in the near surface region is accounted for the major improvement in the PL emission.

© 2009 Elsevier B.V. All rights reserved.

## 1. Introduction

Zinc oxide (ZnO) has attracted much attention in recent years due to its applications for various optoelectronics devices including antireflection coating, electrodes in solar cells [1], gas sensors [2], varistors [3], and surface acoustic wave devices [4], etc. The advantage of this material is a direct band-gap of 3.3 eV and extremely large exciton binding energy of about 60 meV, high chemical stability and UV laser action at room temperature [5]. However, the properties of the as-grown crystals are largely controlled by intrinsic defects such as oxygen vacancies and zinc interstitials in ZnO. ZnO generally emits three luminescence bands in the UV, green and red regions. For lasing applications, high quality single crystal with strong UV emission is desirable, while the green/red emission is not desirable. At present various mechanisms for the green emission has been proposed such as oxygen vacancies [6], oxygen antisite defects [7] or zinc vacancy defects [7]. The red emission is related to the lattice imperfections [8].

Ion implantation is a powerful tool to control and modify the properties of crystals at precise depths below the surface. ZnO shows more resistance to radiation damage in comparison with Si, GaAs, and GaN. Oxygen vacancies in ZnO play a significant role in controlling the optical and electronic properties of ZnO. Since as-grown crystals often contains oxygen vacancies, oxygen implantation in the near surface region is expected to compensate for the oxygen vacancy sites and improve the structure of ZnO crystal. Very little work has been done on the effect of oxygen ion implantation on the near surface region of ZnO single crystals. Zhao et al. [9] studied the effect of O and Zn implantation on the deep level emission of ZnO and they identified the deep level emissions related  $V_{\text{Zn}}$  and  $O_{\text{Zn}}$ . Zhong detected a novel transition at emission energy of 3.08 eV at 77 K and attributed it to  $O_{\text{Zn}}$  defect [10]. However, no improvement in the UV emission was reported from these O implanted ZnO samples. In this work, low energy oxygen implantation induced improved crystallinity and optical properties of surface modified ZnO single crystals are studied. Undoped ZnO (0 0 0 1) single crystal wafers are implanted with 100 keV oxygen ions at a dose of  $5 \times 10^{13}$  and  $5 \times 10^{14}$  cm<sup>-2</sup> and subsequently annealed at 500 and 600 °C in oxygen ambient. The as-implanted and annealed ZnO wafers are studied by X-ray diffraction (XRD), Rutherford back scattering spectrometry (RBS), channeling, Raman, photoluminescence (PL), and Fourier transform infrared spectroscopy (FTIR) measurements.

<sup>\*</sup> Corresponding author. Fax: +91 361 2582749.  
E-mail address: [giri@iitg.ernet.in](mailto:giri@iitg.ernet.in) (P.K. Giri).

## 2. Experimental details

For the present study, undoped ZnO single crystal wafers of n-type conductivity and (0 0 0 1) orientation were procured from SPC Goodwill, Russia. Ion implantation was carried out at room temperature with 100 keV O<sup>+</sup> ions at doses  $5 \times 10^{13}$  and  $5 \times 10^{14}$  cm<sup>-2</sup> using a 150 kV Gaseous Ion Implanter with a RF ion source. Post-implantation annealing was performed in oxygen gas ambient at temperature 500 °C for 10 min and then at 600 °C for 1 h. To avoid possible out diffusion of oxygen atoms from the ZnO surface, low temperature and short duration annealing was chosen. RBS and channeling measurements were performed with 2 MeV He ions from a 1.7 MV Tandem accelerator. Raman spectra were recorded in the backscattering geometry using vertically polarized 488 nm Argon-ion laser beam, double grating monochromator and cooled photomultiplier tube. PL measurements were made at room temperature using a 325 nm He-Cd laser along with a Jobin-Yvon T64000 spectrometer equipped with a cooled charged coupled detector. FTIR measurements were made using a PerkinElmer FTIR spectrometer.

## 3. Results and discussion

Fig. 1 shows a set of Raman spectra for the virgin ZnO and O<sup>+</sup> implanted ZnO wafer. Fig. 1(a) shows that the virgin wafer as well as the as-implanted wafer exhibit  $E_2^{high}$ ,  $E_{2H-2L}$  Raman modes at 438.9 and 333 cm<sup>-1</sup>, respectively [11]. There is apparently a small reduction in Raman intensity of the  $E_2^{high}$  mode after low dose O<sup>+</sup> implantation in ZnO. The small peak at 206 cm<sup>-1</sup> is common to unimplanted and implanted samples and it is usually attributed to the intrinsic defects in the ZnO crystals [12]. In addition to the commonly observed Raman modes, we notice emergence of a strong peak at  $\sim 100$  cm<sup>-1</sup> after implantation and this mode is attributed to the  $E_2^{low}$  mode of ZnO crystal [13]. Fig. 1(b)–(d) shows the relative change in FWHM (full width at half maximum) of the most prominent  $E_2^{high}$  mode before and after implantation. It is interesting to note that FWHM ( $\Delta\nu$ ) of the  $E_2^{high}$  mode first decreases upon implantation (with dose =  $5 \times 10^{13}$  cm<sup>-2</sup>) from 7.89 to 6.63 cm<sup>-1</sup> and then increases to 7.78 cm<sup>-1</sup> with

implantation dose  $5 \times 10^{14}$  cm<sup>-2</sup>. The reduced FWHM indicates lowering of lattice strain after implantation. However, at high dose implantation strain increases, as indicated by the small blue shift of the  $E_2^{high}$  mode (see Fig. 1(d)). Thus, it is evident from Raman analysis that as-implanted ZnO wafers have reduced lattice strain and perhaps improved crystal structure. Raman studies of these samples after 600 °C annealing show that FWHM of the  $E_2^{high}$  mode is again lowest for the low dose implanted samples. Note that  $E_2^{high}$  peak at 438.9 cm<sup>-1</sup> is not symmetric and requires two Lorentzian peaks to fit the experimental data. The low frequency component of the peak is very broad and relatively weak. Although it's not clear about the origin of this low frequency component, it may be related to disorder in the ZnO lattice. Our studies indicate that the ion implantation induced lattice damage may not have fully recovered even after two-step annealing (up to 600 °C), as the Raman intensity of the annealed sample is slightly lower than that of the virgin ZnO wafer. However, lattice strain is reduced in low dose implanted sample as compared to the virgin sample. Similar observation was made from X-ray diffraction line shape analysis of implanted samples after annealing.

The crystal quality of the virgin and as-implanted ZnO wafers was further studied using RBS channeling analysis. Fig. 2 shows that the channeling yield ( $\chi_{min}$ ) of the virgin ZnO wafer is more than 20%, which is quite high, and it increases to  $\sim 33\%$  with implantation doses, as expected. The high value of  $\chi_{min}$  in the virgin sample indicates that the as-grown ZnO crystals contain a lot of intrinsic defects, in particular, of interstitial nature. Usually zinc interstitial, oxygen vacancies or antisite defects are known to be present in the as-grown ZnO crystals. The  $\chi_{min}$  is expected to decrease drastically upon post-implantation annealing, as a result of defect annealing and atomic rearrangements. Fig. 3(a) shows the random and aligned RBS spectra of the virgin ZnO and as-implanted ZnO. The random spectra of the low-dose-implanted sample and the virgin sample are almost identical, indicating very nominal change in the crystalline quality and composition of the sample at the near-surface region. On the other hand, high dose implanted samples show strong change in the composition in the near-surface region of the sample. Fitting of the RBS data (using standard RUMP program) for high dose implanted sample clearly

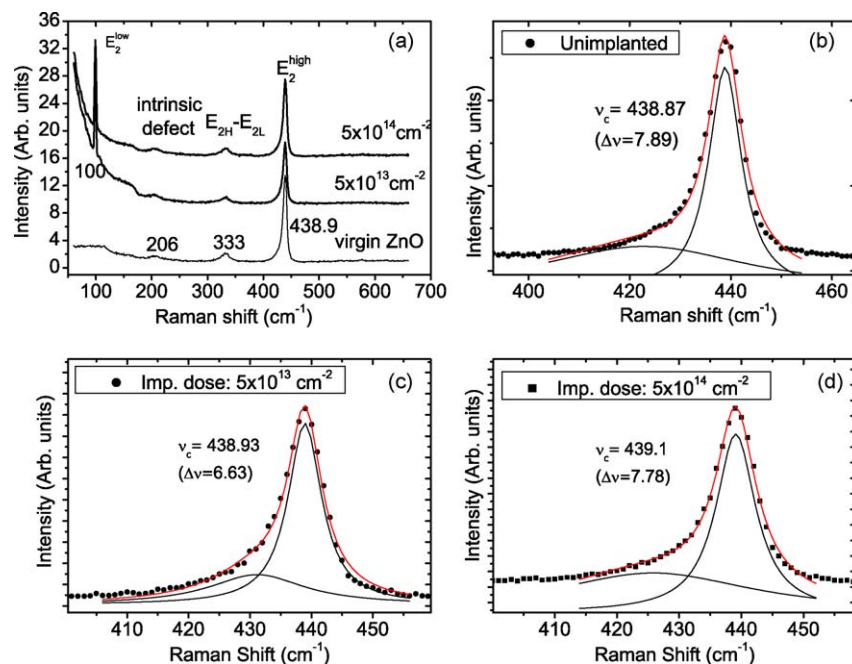


Fig. 1. (a) Raman spectra of the virgin ZnO and as-implanted ZnO wafer implanted with O ions at two different doses. (b)–(d)  $E_2^{high}$  mode peak is fitted (solid line) with Lorentzian line shape to extract the FWHM for different samples. Extracted peak position ( $\nu_c$ ) and FWHM ( $\Delta\nu$ ) for the major peak each case are shown in cm<sup>-1</sup> unit.

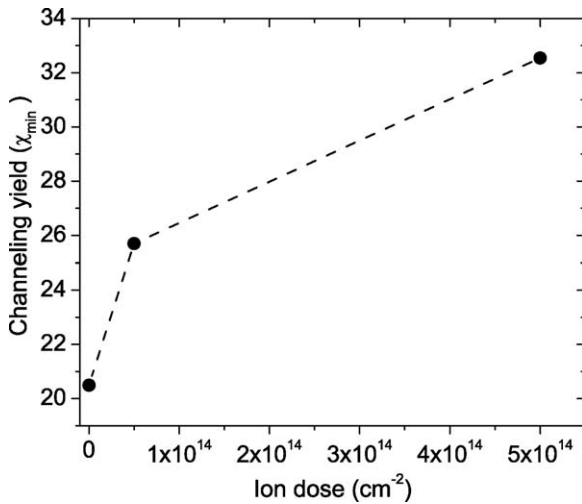


Fig. 2. RBS channeling yield ( $\chi_{\min}$ ) as a function of O ion dose for ZnO crystal.

indicated that oxygen concentration is quite high as compared to the Zn concentration on the top surface layer ( $\sim 190$  nm) of implanted ZnO. It also requires certain amount of roughness on the surface layer to fit the experimental data. Upon annealing at  $600^\circ\text{C}$ , the Zn:O stoichiometry improves due to diffusion of oxygen atoms. It is clear from Fig. 3(b) that crystalline quality improves

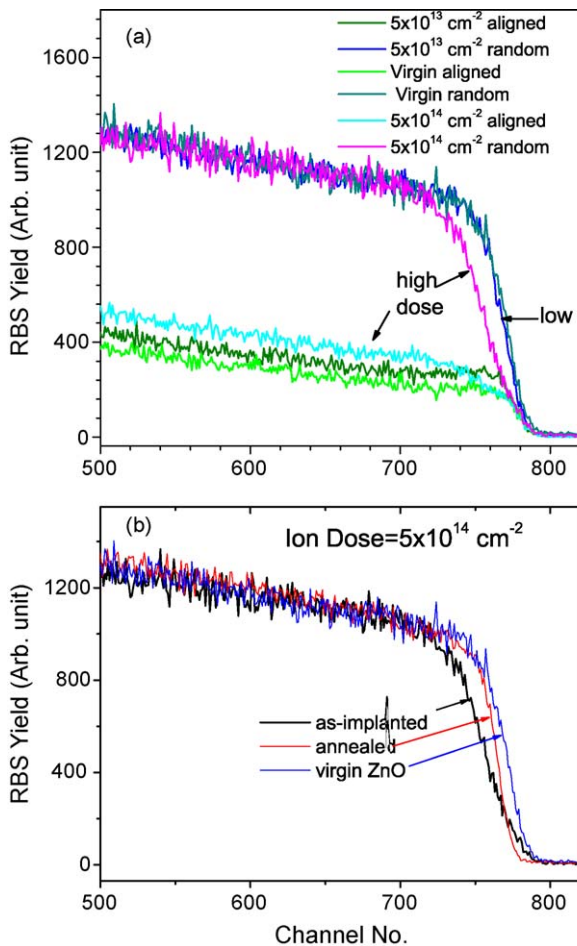


Fig. 3. (a) Random and aligned RBS spectra of the virgin and implanted ZnO crystals before post-implant annealing. (b) Comparison of the RBS spectra (random) for the virgin ZnO, as-implanted ZnO and annealed ZnO wafer for implantation dose  $5 \times 10^{14} \text{ cm}^{-2}$ .

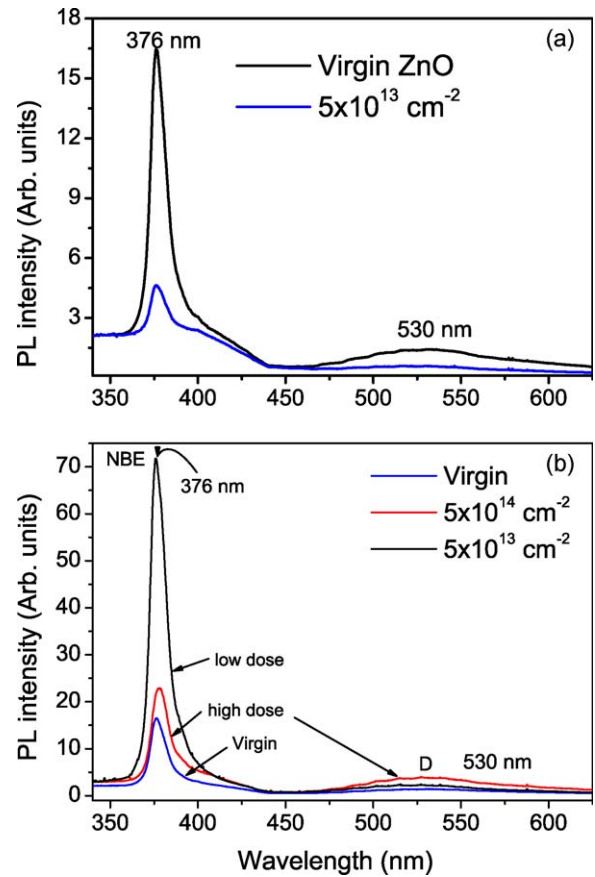


Fig. 4. Room temperature PL spectra of the: (a) virgin and as-implanted ZnO wafer after low dose O implantation; (b) comparison of PL spectra virgin and implanted (low dose and high dose) wafers after two-step annealing at  $600^\circ\text{C}$ . A major improvement in the PL spectra of the low-dose implanted ZnO sample is noteworthy.

after annealing as evidenced by sharper rise of the Zn edge in RBS spectra. Similarly, a major improvement in crystal structure is expected to take place in low dose implanted ZnO wafer.

The effect of ion-implantation and annealing was studied on the room temperature photoluminescence of ZnO; in particular, it's influence on the excitonic UV emission peak intensity. Fig. 4(a) shows the comparison of the PL spectra of the virgin and low-dose as-implanted ZnO wafers. The major UV emission peak at 376 nm is due to excitonic recombination at the near band-edge (NBE) of ZnO [14] and the low intensity broad peak at  $\sim 530$  nm (D-band) is due to intrinsic defects in ZnO. Fig. 4(a) shows that there is a drastic reduction of the NBE emission peak intensity upon implantation of the ZnO wafer. Implantation of energetic ions causes lattice damage and creates varieties of point defects that act as a non-radiative channel to the excitonic NBE emission and this is responsible for the reduced intensity of the NBE peak. This reduction in PL emission is much more severe in case of high dose implanted sample (not shown), where no NBE emission was detectable in the as-implanted ZnO. However, after two-step annealing the point defects are expected to be annealed out to a good extent, though complete recovery of the lattice damage is expected to occur at a higher temperature of annealing. Fig. 4(b) shows the comparison of the PL spectra for the virgin and post-implant annealed ZnO samples. It is evident from the plotted data that after  $600^\circ\text{C}$  annealing, the low dose implanted samples show a major improvement in the intensity of NBE emission with respect to that of the virgin sample. In high-dose implanted sample, the improvement in NBE emission is also present, but to a lesser extent. This major improvement in the NBE emission after low

dose oxygen implantation of ZnO is an important new observation and this can be considered as a milestone achieved for improving the crystal structure and optical properties of ZnO. Since the as-grown ZnO crystals usually have oxygen vacancies, the implanted oxygen ions are expected to fill the vacancies and reduce the lattice strain. This is indeed been achieved in this study as evidenced by our Raman and RBS data. Note that most of the earlier studies have attempted relatively high dose ion implantation for modifying the ZnO structure, since ZnO is a better radiation-resistant material. However, at high doses ion-generated defects and lattice damage are not annealed out at such low temperature (600 °C). The defects primarily act as non-radiative recombination centre and PL emission is usually quenched out. However, low-dose self-ion implantation combined with post-implant annealing produces improved crystal structure with fewer defects and as a result NBE emission is drastically enhanced. Since D-band emission is not desirable for applications in light emitting devices, we monitored the relative change of NBE peak intensity with respect to D-band intensity in all three samples. The intensity ratio of NBE/D-band goes up to 50 (for low dose sample) from initial value of 10 and then reduces back to  $\sim 10$  for high dose sample. Thus there is five-fold enhancement of the UV emission intensity is observed in low dose oxygen implanted ZnO. Note that the two-step annealing was necessary to achieve the enhanced PL emission from oxygen implanted ZnO. This is primarily attributed to reduction in oxygen vacancy concentration and improved crystal structure in ZnO, which reduces the non-radiative channels for recombination of photo-excited carriers. Thus the PL intensity is increased several fold. It may be noted that some studies have reported improved PL emission from thermally annealed ZnO crystals by heating in oxygen environment. However, enhancement is much less compared to the drastic improvement reported here. We find that it is the combined oxygen implantation and post-implant annealing in oxygen ambient (at moderate temperature) that result in the major improvement in the NBE emission from ZnO.

This major improvement in the NBE emission after low dose oxygen implantation of ZnO is of enormous significance for achieving improved light emitting devices made from ZnO single crystals. As-grown ZnO single crystals usually contain large concentrations of intrinsic defects. Due to presence of these defects, the as-grown crystals pose several challenges for the fabrication of devices with high reliability and long lifetime. It may be noted that available method of growing ZnO crystal is also quite expensive. However, this study demonstrates that quality of the as-grown crystals can be improved to large extent by low dose ion-irradiation followed by thermal annealing. Note that previous studies on O implanted ZnO have reported a new PL emission band that was attributed to oxygen antisite defects. Since our studies are performed with relatively low doses, defects do not dominate the PL spectra in our case. Hence, improvement in the NBE emission has been achieved, even with such low temperature annealing.

We further used FTIR spectroscopy to monitor the change in vibrational modes of ZnO after oxygen implantation followed by annealing. In Fig. 5, FTIR spectrum of the virgin ZnO is compared with that of the implanted ZnO. The virgin sample shows Zn–O bending and Zn–O stretching modes at 473 and 527  $\text{cm}^{-1}$ , respectively. Implanted ZnO shows a change in the stretching mode frequency ( $527 \text{ cm}^{-1} \rightarrow 552 \text{ cm}^{-1}$ ) indicating some modification of the bonding upon ion implantation. As the implanted oxygen fills the vacant sites in the ZnO crystal and crystal structure improves upon annealing, the Zn–O stretching mode frequency shifts to higher energy. Thus the observation from Raman, PL and FTIR are consistent regarding the improvement of the surface region of ZnO crystal achieved by low energy (100 keV) and low dose ion implantation. SRIM calculation shows that implanted

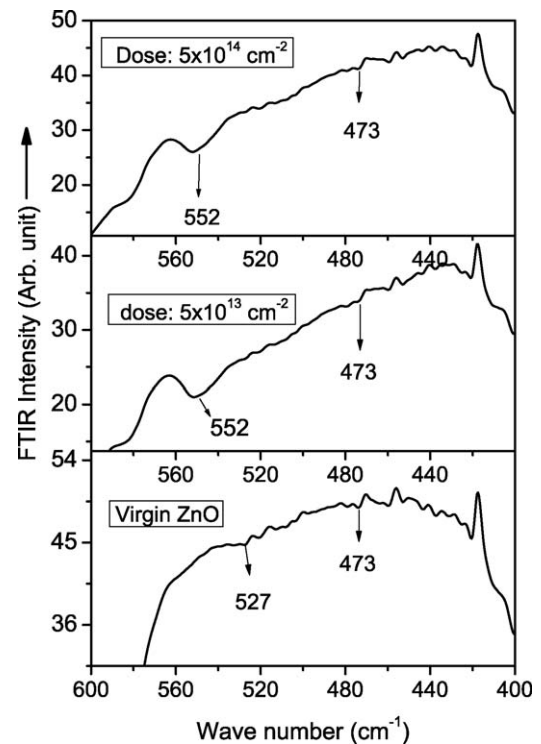


Fig. 5. FTIR spectra of the virgin and implanted ZnO crystals subsequent to post-implant annealing. Important Zn–O stretching and bending modes are denoted in  $\text{cm}^{-1}$  unit.

oxygen has a longitudinal range of  $\sim 150$  nm from the surface and straggling of  $\sim 58$  nm, thus amounting to modification of top  $\sim 200$  nm of the ZnO crystal. From RBS analysis of the implanted ZnO, we have found that composition and crystal structure of the top 190 nm is modified by the oxygen irradiation. Thus the modification of the near-surface region of ZnO results in the improved structural and optical properties of the ZnO crystal. As noted earlier, recovery of the lattice damage is not complete after 600 °C annealing of the implanted ZnO. Higher temperature annealing would be required to achieve complete healing of the damage cascade produced by ion implantation. More studies are underway to study the systematic of the improvement in the structural and optical properties of ZnO single crystal.

#### 4. Conclusions

We have studied the effect of low-energy low-dose oxygen implantation induced changes in the crystallinity and optical properties of ZnO single crystal wafer. The energy and ion doses are chosen such that only near surface region of the crystal is modified. Raman line shape analysis clearly indicates reduced lattice strain after low dose implantation of ZnO. Channeling studies show that virgin ZnO wafer has unusually high  $\chi_{\min}$  that further increases with ion implantation. After two step annealing, RBS studies show improved crystallinity in the implanted samples as compared to the virgin wafer. Raman analysis shows that besides the reduced line width of the  $E_2^{\text{high}}$  mode, strong  $E_2^{\text{low}}$  Raman mode of ZnO appears after oxygen implantation. As-implanted samples show drastic quenching of the near band-edge (NBE) PL band due to defects (traps) created by the implantation. However, after two stage annealing, the low dose implanted sample show a major improvement in the NBE PL emission at  $\sim 376$  nm and a five-fold increase in intensity ratio of NBE band to D-band. Implantation induced changes in the composition and improved crystallinity in the near surface region

is accounted for the major improvement in the PL emission. FTIR studies also show corresponding changes Zn–O stretching modes after implantation and subsequent annealing.

### Acknowledgements

This work was carried out with the financial support from UGC-DAE CRS project. We are thankful to Dr. B K Panigrahi and Dr. K G M Nair for providing facilities for ion-implantation and RBS scattering studies.

### References

- [1] T.W. Hamann, A.B.F. Martinson, J.W. Elam, M.J. Pellin, J.T. Hupp, *Adv. Mater.* 20 (2008) 1560.
- [2] K.S. Weissenrieder, J. Muller, *Thin Solid Film* 300 (1997) 30.
- [3] M.S. Ramanchalam, A. Rohatgi, W.B. Carter, J.P. Shaffer, T.K. Gupta, *J. Electron. Mater.* 24 (1995) 413.
- [4] W.-C. Shih, M.-S. Wu, *J. Cryst. Growth* 137 (1994) 319.
- [5] D.M. Bagall, Y.F. Chen, Z. Zhu, T. Yao, S. Koyama, M.Y. Shen, T. Goto, *Appl. Phys. Lett.* 70 (1997) 2230.
- [6] T.M. Børseth, B.G. Svensson, A.Yu. Kuznetsov, P. Klason, Q.X. Zhao, M. Willander, *Appl. Phys. Lett.* 89 (2006) 262112.
- [7] B. Lin, Z. Fu, Y. Jia, *Appl. Phys. Lett.* 79 (2001) 943.
- [8] B.J. Pierce, R.L. Hengehold, *J. Appl. Phys.* 47 (1976) 644.
- [9] Q.X. Zhao, P. Klason, M. Willander, H.M. Zhong, W. Lu, J.H. Yang, *Appl. Phys. Lett.* 87 (2005) 211912.
- [10] H. Zhong, X. Chen, L.Z. Sun, W. Lu, Q.X. Zhao, M. Willander, *Chem. Phys. Lett.* 421 (2006) 309.
- [11] N. Ashkenov, B.N. Mbenkum, C. Bundesmann, V. Riede, M. Lorenz, D. Spemann, E.M. Kaidashev, A. Kasic, M. Schubert, M. Grundmann, G. Wagner, H. Neumann, *J. Appl. Phys.* 93 (2003) 126.
- [12] B. Cheng, Y. Xiao, G. Wu, L. Zhang, *Appl. Phys. Lett.* 84 (2004) 416.
- [13] C.A. Arguello, D.L. Rousseau, S.P.S. Porto, *Phys. Rev.* 181 (1969) 1351.
- [14] K. Thonke, Th. Gruber, N. Teofilov, R. Schonfelder, A. Waag, R. Sauer, *Physica B* 308–310 (2001) 945.